

Enhanced atmospheric pollutants strengthened winter convective mixing and phytoplankton blooms in the northern Arabian Sea

B. Sridevi¹ and V.V.S.S. Sarma^{1,2,*}

¹CSIR-National Institute of Oceanography, 176 Lawsons Bay Colony,
Visakhapatnam – 530017, India

²Academy of Scientific and Innovative Research, Ghaziabad, India

* Corresponding author (sarmav@nio.org)

Abstract

The recent increase in atmospheric pollutants (aerosols) over the northern Indian Ocean due to an increase in industrial activity in South and Southeast Asia decreased air temperature (AT) leading to the strengthening of winter convective mixing and promotion of phytoplankton blooms in the northern Arabian Sea (AS). To test this hypothesis, the variability in meteorological and surface ocean properties was analyzed for a period of 4 decades (1979-2018) in the northern AS. The total and anthropogenic aerosol optical depth (AOD) increased at a rate of 0.05 and 0.07 per decade respectively in the recent decades associated with a decrease in air temperature (AT) over the northern AS during winter. The estimated decrease in AT due to increasing AOD accounts for 0.18°C over the AS and it is close to that of the mean decrease in AT from 1994 to 2018 of 0.25°C. This increased the difference in temperature between the sea surface and atmosphere and enhanced specific humidity in the atmosphere resulting in the strengthening of convective mixing in the northern AS as evidenced by the deepening of the depth of 20°C isotherm in the recent decades during winter. Enhanced nutrient concentration and phytoplankton biomass were observed in the photic zone during winter further confirming that convective mixing strengthened in the recent decades in the northern AS than hitherto hypothesized as weakening due to the warming of the Eurasian landmass. The enhanced nutrients supported diatoms blooms, which are prey for *Noctiluca scintillans* to initiate the bloom in the AS in the recent decades.

Keywords: winter convective mixing, Atmospheric dust, net heat flux, nutrients inputs, Arabian Sea.

Plain Language Summary

Atmospheric pollution is ever-increasing over the northern Indian Ocean leading to decreasing solar radiation resulting in a decrease in atmospheric temperature. This led to an increase in temperature difference between sea surface and atmosphere which triggers convective mixing and supply of nutrients to the surface. The enhanced nutrients support the formation of phytoplankton blooms and a decrease in oxygen concentrations in the subsurface waters. This work suggests that atmospheric pollution modifies oceanic mixing patterns and increases food for heterotrophs in the northern Arabian Sea.

1. Introduction

Atmospheric aerosols play a pivotal role in influencing global climate through modifications in the radiation budget (IPCC, 2001). Aerosol optical depth (AOD) indicates the absorption of sunlight-induced by aerosols (haze) and direct measurement of aerosol loading, which contributes to rating global climate change (Zhao et al., 2008). A rapid increase in AOD is reported from 2001-to 2011 by $\sim 4\%/y$ over the Indian subcontinent (Krishna Moorthy et al., 2013; Srivastava, 2017). Since the northern Indian Ocean has been covered on three sides by an Asian landmass, where one-third of the global population is dwelling close to the coast, more anthropogenic aerosols are produced (Rastogi et al., 2020). The seasonal variations in winds support the seasonal migration of the Inter-Tropical Convergence Zone (ITCZ) allowing to spread of pollutants over the Indian Ocean (Ramanathan, 1996). In the past few decades, emissions from various pollutants and their components in the fast-growing and expanding countries (such as India and China) are increased rapidly due to enhanced industrial activity, motorization and agricultural practices (Kurokawa and Ohara, 2020). Zhang and Reid (2010) reported the highest rate of increase in AOD per decade over the Bay of Bengal, followed by coastal China Sea, and Arabian Sea (AS) between 2000 and 2009 and it was found that the rate is further increased in the recent decades (2010-2019; Yadav et al., 2021) in the BoB. Dong et al. (2014) reported that significant cooling of atmospheric temperature due to aerosols over the northern Indian Ocean due to a decrease in incoming radiation to the lower atmosphere.

The AS experiences a seasonal reversal in surface winds that blow from the northeast (NE) during boreal winter resulting in the transport of pollutants from the Indo-Gangetic Plain (IGP) to over northern AS (Ramanathan et al., 1996) leading to a decrease in incoming short-wave radiation and cooling of the lower atmosphere by about 4°C (Ramanathan et al., 2002). In addition to this, the NE winds are cold and dry resulting in an increase in evaporation over the northern AS leading to the high surface density that triggers convective mixing (Madhupratap et al., 1996; Dickey et al., 1998). The strong convective mixing is also supported by a rapid decrease in specific humidity of air from 19 g/kg in October to 10 g/kg in December (Prasad and Kumar, 1996). The crucial parameters to set convective mixing are the differences in sea-air temperature, specific humidity of air and wind speed (Tomczak and Godfrey, 1994).

A deep mixed layer of >100 m was reported during winter associated with convective mixing in the northern AS resulting in the entrainment of nutrient-rich waters into the photic layer (de Sousa et al., 1996; Morrison et al., 1998) that triggers phytoplankton blooms (Bhattathiri et al., 1996; Barber et al., 2001). An increase in export production (Buesseler et al., 1996) and intense oxygen minimum zone (OMZ; de Sousa et al., 1996) and high surface pCO₂ levels (Sarma et al., 1998) were reported associated with convective mixing. Banse et al. (2014) reported depletion of oxygen in the OMZ at the rate of 0.19 μM/y during winter for the past four decades and potential reasons for such changes are unclear. Thicker and intense OMZ was reported in the northern AS during winter due to high phytoplankton biomass and export flux supported by convective mixing (de Souza et al., 1996; Morrison et al., 1998). Therefore, variations in the strength of convective mixing play an important role in the biogeochemistry of oxygen, carbon and nitrogen cycling in the northern AS. Recently, Goes et al. (2020) reported that warming of the Eurasian land surface due to global warming increased air temperature resulting in a weakening in winter convective mixing between 1980 and 2018 resulting in the occurrence of *Noctiluca scintillans* blooms. Diatoms are the preferred prey of green *Noctiluca scintillans* and often develop following diatom blooms (Kiorboe and Titelman, 1998; Dwivedi et al., 2015). Gomes et al. (2008) reported the occurrence of *Noctiluca* blooms during spring intermonsoon (March to May). They found that mesoscale eddies in the western AS contribute to the genesis and dispersal of *Noctiluca* blooms from the Gulf of Oman into the central AS. Xiang et al. (2019) found the occurrence of *Noctiluca Scintillans* blooms in the northern Arabian Sea, off Pakistan, during February. They reported that stable water column, low silicate concentrations, high light conditions and accumulation of organic nutrients provided favourable conditions for their growth. This is consistent with similar interpretations given by several investigators (Prakash et al., 2017; Lotiliker et al., 2018; Wasmund et al., 2013; Sarma et al., 2019). The *Noctiluca* blooms formations involve four different stages: 1) an increase in nutrients leading to the formation of phytoplankton blooms (say diatoms), 2) due to an increase in the availability of prey, *Noctiluca* abundance increases, 3) the exponential growth of *Noctiluca* occurs by through reproduction and 4) decrease in abundance caused by either lack of prey, consumption by larger predators or carried away by winds (Miyaguchi et al., 2006; Baek et al., 2009; Harrison et al., 2011; Gomes et al., 2014). Gomes et al. (2014) found that *Noctiluca* can able to survive in the absence of nutrients and external prey for a period of about a year, however, they cannot bloom under such

conditions. Gomes et al. (2018) reported, based on the laboratory experiments on *Noctiluca* isolated from the Arabian Sea, that *Noctiluca* prefers *Peridinium foliaceum* and the pennate diatom *Phaeodactylum tricornutum* as food for their growth. Therefore, before *Noctiluca* blooms, diatoms abundance enhances due to an increase in nitrate, phosphate and silicate concentrations caused by winter convective mixing that act as prey for *Noctiluca*. Gomes et al. (2014) observed that the growth of *Noctiluca* enhances in the low oxygen compared to oxic conditions. Since convective mixing brings low oxygen and nutrient-rich waters from the subsurface, the conducive conditions prevail for *Noctiluca* to bloom. This is the reason the green *Noctiluca* blooms occur at the end of the winter (February), when winter convective mixing weakens and stratification occurs due to the westward flow of West India Coastal Currents and change in direction of winds (Prakash et al., 2017; Sarma et al., 2019; Xiang et al., 2019). The diatom bloom is observed in the western region of Northern AS and proceeds towards the east followed by the development of green *Noctiluca* blooms (Kiorboe and Titelman, 1998; Dwivedi et al., 2006; 2015). Therefore, the enhanced convective mixing supplies more nutrients resulting in enhanced diatom blooms and therefore *Noctiluca* bloom's intensity (Gomes et al., 2018). In contrast, the weakening of convective mixing may result in the pumping of fewer nutrients to the surface and low diatom biomass, which may lead to a decrease in prey availability and a decrease in *Noctiluca* biomass (Gomes et al., 2018). Goes et al. (2020) reported that winter convective mixing is weakened in the recent decade, in contrast, *Noctiluca* blooms were intensified. Since convective mixing and *Noctiluca* blooms were inter-connected, as the intensity of mixing determines the prey concentration, a more robust explanation is required to understand potential reasons responsible for the recent increase in *Noctiluca* abundance in the northern AS. We made here an attempt to understand the long-term variability in winter convective mixing and phytoplankton biomass in the AS over a period of 4 decades (1979 - 2019) by analyzing data from remote sensing, model and Argo floats data.

2. Data and Methodology

Data from multiple sources were utilized to carry out the present study. ERA-Interim monthly reanalysis data of Air Temperature (AT), Sea Surface Temperature (SST), and winds were taken from ECMWF (European Centre for Medium-Range Weather Forecasts) with a grid resolution of $0.25 \times 0.25^\circ$ during the period 1979 to 2018.

Total aerosol optical depth (AOD) data at 470 nm, 550 nm, and 860 nm wavelengths were obtained from moderate resolution imaging spectroradiometer (MODIS) Terra satellite collection 6.1 and level 3 from 2001 to 2019 (<https://ladsweb.modaps.eosdis.nasa.gov/search>) at 1 x 1° resolution. The fine mode fraction of AOD was computed following Levy et al (2013). The anthropogenic fraction of AOD from total AOD was estimated following Kaufman et al. (2005a, b). The complete procedure and assumptions used in these estimations were given in Yadav et al. (2021). The errors in the total AOD and anthropogenic AOD are ±0.03+5% of AOD and ±0.05+8% of AOD respectively (Wei et al. (2019).

Mixed layer depth (MLD), defined as the depth where the buoyancy difference with respect to the surface is equal to 0.03 cm s⁻², is obtained from the Global Ocean Data Assimilation System (GODAS) with a grid of 1° x 1/3° resolution for the period 1980 to 2018. Reanalysis data of salinity and D20 was downloaded from the Asia-Pacific Data Research centre (http://apdrc.soest.hawaii.edu/data/data.php?discipline_index=2) during the period 1979 to 2018 with monthly interval and 1 x 1° grid spatial resolution. This data was provided by European Centre for Medium-Range Weather Forecast (ECMWF) estimates the oceanic state via the operational system OCEAN5. The OCEAN5 system was used for the production of Ocean Reanalysis System 5 (ORAS5) which provides the historical ocean state from 1979 to the present. Specific humidity of air, latent heat flux and net heat flux data with a resolution of 1° x 1° grid for the period 1970-2019 were taken from the newly developed global Tropical air-sea heat fluxes (TropFlux; Kumar et al., 2012). Monthly averaged chlorophyll-a (Chl-a) data with a resolution of 9 km were obtained from the MODIS-Terra satellite (from 2001 to 2019) (<https://oceandata.sci.gsfc.nasa.gov>).

The difference between SST and AT (δT) is calculated to understand whether sensible heat transfer is from the ocean to the atmosphere or *vice versa*. Positive δT indicates loss of heat through sensible heat flux from the sea surface. The saturation-specific humidity of air (q_s) at sea surface temperature is estimated with the following equation:

$$q_s = \frac{(0.622 * e_s)}{(p - 0.378 * e_s)}$$

p is surface pressure and e_s is the saturation vapour pressure of air at SST and it is estimated using $e_s = T_d^A * 10^{(B + C/T_d)}$ where T_d is water temperature (or SST) in Kelvin and the constants $A = -4.928$; $B = 23.55$; and $C = -2937$. The difference in specific humidity ($\delta q = q_s - q_a$) is calculated as the saturation specific humidity of water (q_s) minus specific humidity of air (q_a) as a proxy to the moisture transfer flux or evaporation across the sea surface. Positive δq indicates the loss of moisture or water vapour through evaporation from the sea surface.

3. Results

3.1. Spatial variations in SST, MLD, and Chl-a in the AS

Figure 1 shows the spatial variability in climatological mean SST, MLD and surface Chl-a during winter. Significant cooling was noticed north of 18°N associated with deepening of MLD and increase in Chl-a (Fig. 1a-c). Madhupratap et al. (1996) reported that significant convective mixing occurs north of 15°N in the AS and its impact decreases towards the south. While we discussed the spatial variability in trends in physical and biogeochemical properties, we analyzed time series variability in the core convective mixing zone of 18-22°N and 62-68°E (shown by a box in Fig. 1) during winter (December, January and February; DJF) to evaluate the long-term changes.

3.2. Spatial variability in long-term trends in AT, SST, and δT

The long-term trends in Air Temperature (AT) during winter displayed strong spatial variability from 1979-to 1993 and 1994-to 2018 in the Arabian Sea (Fig. S1a-b). A significant warming trend of 0.5°C/decade in AT was observed in the northern AS from 1979 to 1993. Even though the increasing trends were noticed in the southern AS but they were statistically insignificant from 1979-to 1993. In contrast, cooling trends (-0.2°C/decade) were noticed in the central and western AS and warming trends in the eastern AS from 1994 to 2018 (Fig. S1a,b). Similarly, the trends in AT and SST were almost uniform from 1979-to 1993 and 1994 to 2018 in the AS. The SST displayed a significant warming trend of 0.3-0.5°C/decade in the entire Arabian Sea from 1979 to 1993, except for a small region in southeastern AS, in contrast, weak cooling trends were noticed in the western AS and warming trends in the eastern AS (Fig. S1c,d). The difference between SST and AT (δT) showed decreasing trends in the northern (north of 12°N) and eastern AS whereas a weak increasing trend in the south of 12°N and southwestern AS is found from

1979 to 1993 (Fig. 2a). In contrast, a strong warming trend was observed off Somalia in the southwestern AS and weak warming trends in the western whereas weak cooling trends in the eastern AS from 1994 to 2019 (Fig. 2b).

3.3 Long-term variability in AT, SST and SSS in the selected region in the northern AS.

AT displayed significant warming trend ($0.59^{\circ}\text{C}/\text{decade}$) from 1979 to 1993 but this trend was insignificant from 1994 to 2018 (Table 1; Fig. 3a). The monthly mean AT from December to February (Supplementary Fig. S2-4; Table 1) displayed a significant increasing trend from 1979- to 1993 ($0.52\text{-}0.60^{\circ}\text{C}/\text{decade}$) and an insignificant trend was noticed from 1994 to 2018 (Fig. 2a; S2-S4). Similarly, an increase in the rate of warming of the sea surface was noticed from 1979 to 1993 ($0.41\text{-}0.69^{\circ}\text{C}/\text{decade}$ mean of $0.54^{\circ}\text{C}/\text{decade}$) and an insignificant trend was observed from 1994 to 2018 (Table 1; Fig.3b and Supplementary Fig. S2-S4). The mean sea-to-air temperature difference ($\delta T = \text{SST-AT}$) during winter displayed an insignificant decreasing trend ($-0.05^{\circ}\text{C}/\text{decade}$) from 1979 to 1993 whereas it increased significantly ($+0.1^{\circ}\text{C}/\text{decade}$) from 1994 to 2018 (Fig. 3c). The winter means SSS decreased at a rate of -0.09 /decade from 1979 to 1993 whereas insignificant trends were noticed from 1994 to 2018 (Fig. 3d) (Table 1; Supplementary Fig. S2-4).

3.4. Long-term variability of wind, mixed layer depth, depth of 20°C isotherm (D20) and heat fluxes

The winter mean trends in windspeed showed decreasing trends in the north and south but a weak increasing trend in the central AS from 1979 to 1993 (Fig. 2c), in contrast, a strong increasing trend in the southwestern AS and a weak increasing trend in the rest of the AS during 1994-2018 (Fig. 2d). The decreasing (shallowing) trend in mixed layer depth ($\sim 5\text{m}/\text{decade}$; Fig. S1e) was noticed in the entire AS except the east coast of India, central and western AS (1979-2018) whereas insignificant trends were noticed during 1994-2018, except in the southern AS, where the significant decrease was observed) (Fig. S1f & Fig. 2d). MLD displayed a significant decreasing trend from 1979 to 1993 ($-7.8 \text{ m decade}^{-1}$) but this trend is statistically insignificant from 1994 to 2018 in the selected region in the northern AS (Table1, Fig. 3f).

The D20 displayed a significant decreasing (shallowing) trend in the entire AS, except in the central AS from 1979 to 1993 whereas a significant increasing (deepening) trend was noticed in the entire AS, except the southwestern region, from 1994 to 2018 (Fig. S1g,h). The D20 did not

display a significant trend in the northern AS but it was deepened at a rate of $\sim 6.7 \text{ m decade}^{-1}$ (Fig. 3e) from 1994 to 2018. In addition to this, the D20 derived from Argo floats data was also compared with model data between 2004-2018 when Argo data are available. The rate of deepening of D20 during 2004-2018 was $17.7 \text{ m decade}^{-1}$ based on Argo's data whereas it was $12.6 \text{ m decade}^{-1}$ by the model during the same period (Fig 3e).

The mean product of saturated minus air specific humidity (δq) during winter showed a decreasing trend in the northern and central AS whereas an increasing trend in the southern AS from 1979 to 2013. In contrast, an increasing trend in the northern and central AS and decreasing trend in the southern AS was noticed from 1994 to 2018 (Fig. 2e,f). The δq did not display a statistically significant trend in the selected region in the northern AS (Table 1, Fig. 3d). The evaporation quantity can be explained through latent heat flux from the sea to the atmosphere and it showed an increasing trend (decrease in evaporation) in the northern AS, and decreasing trend (increase in evaporation) from 1994 to 2018 (Fig. 2g,h). The trends in winter mean net heat flux displayed an increasing trend (decrease in heat loss) during winter between 1979 and 1993 ($11.07 \text{ W m}^{-2} \text{ decade}^{-1}$) with a relatively lower increasing trend in February ($1.4 \text{ W m}^{-2} \text{ decade}^{-1}$) than in December and January ($16.45\text{-}17.69 \text{ W m}^{-2} \text{ decade}^{-1}$) whereas it was decreased (increased net heat loss) between 1994 and 2018 ($-3.24 \text{ W m}^{-2} \text{ decade}^{-1}$) (Table 1).

3.6. Long-term variability in AOD

Total AOD in the AS varied between 0.1 and 0.5 (Fig. 1d) and it was relatively higher during winter and lower during summer. Increasing trends in both total and anthropogenic AOD were noticed in the northern AS from October to February (Fig. 4 and 5). The long-term trends in the total and anthropogenic AOD during December, January, February and the mean of winter displayed a significant increasing trend in the selected region (Fig. 6). Wind speed from October to February is from the northeast (terrestrial to marine) whereas wind blows from marine to terrestrial during other months (Fig. 4). The rate of increase in total and anthropogenic AOD varied between 0.04 to 0.07 and 0.03 to 0.08/decade from December to February with winter mean rate of increase of 0.05 and 0.07/decade respectively (Fig. 6).

3.7. Long-term trends in Chl-a

The spatial distribution of Chl-a during winter in the AS was shown in Figure 1c, which displayed significant meridional variability. Higher ($>1 \text{ mg m}^{-3}$) Chl-a concentration was

observed in the north of 18°N and steeply decreased by 10 times towards the south (south of 18°N). The increasing trends in Chl-a were observed in the northwestern AS whereas the decreasing trend was in the northeastern AS. The trends in the entire AS were statistically insignificant (Supplementary Figure S5). Within the selected box, the seasonal mean surface Chl-a did not show any statistically significant trends between 2001 and 2019 (Table 1, Fig. 3g).

4. Discussion

4.1. Potential mechanisms responsible for decadal variability in winter latent and net heat flux in the northern AS

Contrasting spatial trends of AT (Fig. S1a-b), SST (Fig. S1c-d), δT (Fig. 2a-b), winds (Fig. 2c-d), δq (Fig. 2e-f), latent (Fig. 2g-h) and net heat flux (Fig. S1i-j) were noticed in winter between 1979 to 1993 and 1994 to 2018. For instance, AT and SST displayed an increasing trend in the entire AS from 1979 to 1993, in contrast, cooling trends in the west and warming trends in the east were noticed between 1994 and 2018. Roxy et. al. (2015) reported $>0.1^\circ\text{C}$ in SST raise per decade between 1901 and 2012 in the summer season (June-September) in southwestern AS. Our study noticed an increase in SST by $0.5^\circ\text{C}/\text{decade}$ between 1979 and 1993 during the winter season suggesting that the rate of warming is not uniform with reference to season and space in the AS.

Though an insignificant rate of warming in AT and SST was noticed during 1994-2018 in the northern AS, the trends in δT were positive (increasing) trends compared to negative trends during 1979-1993 suggesting that the sea surface was warming over the atmosphere during former than latter period (Fig. 2a,b). Weakening of winds associated with decreasing trends in δq resulting in increasing rates in latent heat flux suggests a decrease in evaporation during 1979-1993 than 1994-2018 (Fig. 2c-h). The net heat flux suggests the ocean lost less heat to the atmosphere from 1979 to 1993 than from 1994 to 2018 (Fig. S1 i-j). These results suggest that the AS lost more heat to the atmosphere during winter in 1994-2018 than in 1979-1993.

The difference in δT from 1979 to 1993 and 1994 to 2018 is mainly caused by variations in the AT. The warming trends in winter mean AT was noticed over the northern AS between 1979 and 1993 ($+0.59^\circ\text{C}/\text{decade}$) and an insignificant cooling trend was observed between 1994 and 2019 ($-0.05^\circ\text{C}/\text{decade}$) indicating a secular decadal variability in AT (Fig. 3a) with relatively

weaker warming during the latter than former period. Kothawale and Kumar (2002) reported warming of AT over the Indian subcontinent at the rate of $+0.27^{\circ}\text{C}$ per decade between 1971 and 2000 and it is consistent with our observations as it falls between 1979-1993 ($+0.59^{\circ}\text{C}/\text{decade}$) and 1994-2019 ($-0.05^{\circ}\text{C}/\text{decade}$). The warming of AT between 1979 and 1993 is consistent with the beginning of industrialization in South and Southeast Asia. Kurokawa and Ohara (2020) estimated long-term historical trends in air pollutants in Asia and noticed a significant increase in air pollution in the past 6 decades. The rate of increase in pollution was at a lower rate between 1970 and 1990 when industrialization was initiated in this region as reflected in the economic situation (<https://www.worldbank.org/>) and rapidly increased from the 1990s to the present. The rate of increase in pollutants over China peaked in 2015 and decreased afterwards whereas the emission from India and other Southeast Asian countries increased along with economic growth and motorization (Kurokawa and Ohara, 2020). Numerous studies revealed that atmospheric aerosols directly affect the surface radiation budget by absorbing and scattering the incoming solar radiation and modifying cloud microphysical properties (Towmey, 1977; Yu et al., 2006; Andreae and Rosenfeld, 2008; Boucher et al., 2013). Recently Sarin et al. (2021) noticed the mean warming of the sea surface by 0.83°C in the central and north-western Bay of Bengal during 2020 (COVID-19 pandemic lockdown period) than the climatological mean of 2003-2019. They estimated that about 30% of this warming was attributed to reduced inputs of atmospheric aerosols. The initial rate of increase in atmospheric pollutants (1979-1993) enhanced AT due to the trapping of outgoing radiation. The rapid increase in pollutants into the atmosphere from 1994 to 2019 leads to the formation of Asian Brown Clouds (Ramanathan et al., 2001) that inhibited part of the incoming radiation to reach the lower atmosphere. The decrease in AT during recent decades (1994-2019) is consistent with an increase in both total ($0.05/\text{decade}$) and anthropogenic AOD ($0.07/\text{decade}$; Fig. 6) and it is slightly higher than that from 2001 to 2009 (0.06 ; Zhang and Reid, 2010). The anthropogenic AOD contributed to ~50-80% of total AOD in the northern AS during winter suggesting that the rapid increase in AOD is contributed by industrial activities over the Indo-Gangetic Plain (IGP; Kumar et al., 2008; Srinivas et al., 2013). Sarin et al. (2021) found that an increase in 1 unit of AOD cools the atmospheric temperature by 1.25°C and 1.64°C in the Equatorial Indian Ocean and Bay of Bengal respectively due to variability in the aerosol loading. The rate increase in AOD between 2001 and 2018 was $0.05/\text{decade}$ (Fig. 6) and it accounts for an increase of 0.125 for 25 years

(1994-2018), assuming the rate is similar between 1994 and 2018. Using the mean of the slope of AOD to SST ($1.4^{\circ}\text{C}/1$ unit AOD) in the Bay of Bengal and Equatorial Indian Ocean, the decrease in AT due to an increase in AOD accounts for 0.18°C over the AS. This is close to that of the mean decrease in AT observed between 1994 and 2018 of 0.25°C (at the rate of $0.01^{\circ}\text{C}/\text{y}$; Fig. S1b). The assumption of slope between AOD and SST from the Bay of Bengal and Equatorial Indian Ocean may be reasonable as the same source of pollutants spread over the northern Indian Ocean.

Recently Goes et al. (2020) observed a decline in the snow cover over the Himalayan region between 1980 and 2016 resulting in increasing trends in AT. Since the period under consideration in Goes et al. (2020) falls between the warming period ($+0.59^{\circ}\text{C}/\text{decade}$; 1979-1993) and the cooling period ($-0.05^{\circ}\text{C}/\text{decade}$; 1994-2019; Table 1), the net trend showed as weaker warming trend. The recent cooling trend over the Indian subcontinent and northern AS was also contributed by a significant increase in the frequency and intensity of extreme weather events, such as cold waves, due to climate change (Pai et al., 2017). The western disturbances play a crucial role in generating cold waves or bringing the winter rainfall over the Himalayan region (Dimri et al., 2015; Ratnam et al., 2016). Pai et al. (2017) noticed that the frequency and intensity of cold waves over the northern Indian subcontinent decreased from 1971-1980 to 1991-2000 whereas it increased in the recent decade (2001-2017). The increase in cold waves may also be partially responsible for the cooling of AT over the Indian subcontinent and the northern Indian Ocean in the recent decade during winter (Pai et al., 2017). Even though global temperatures are increasing, both increases in atmospheric aerosols and cold waves suppress the rise in the magnitude of long-term trends in AT over the Indian subcontinent, and the northern Indian Ocean, including the Eurasian Land surface, during winter (Fig. 3a,b). Dong et al. (2014) found that about 50% of the warming due to greenhouse gases was cooled by atmospheric aerosols in the northern Indian Ocean during recent decades.

Since $\sim 90\%$ of heat due to global warming is accumulated in the oceans (IPCC, 2013), SST was increased over the past several decades. Warming of SST was noticed between 1979 and 1993 ($+0.54^{\circ}\text{C}/\text{decade}$) than 1994-2019 ($+0.04^{\circ}\text{C}/\text{decade}$; Fig. 3b) and it is consistent with the higher atmospheric warming rate ($+0.59^{\circ}\text{C}/\text{decade}$) during former decades (1979-1993) than latter ($-0.05^{\circ}\text{C}/\text{decade}$; Fig. 3a). The sea-to-air temperature difference (δT) explains the strength of

winter convective mixing. If this difference is more positive, then the ocean loses more heat to the atmosphere and vice versa for negative (Kumar and Prasad, 1996). The δT displayed a negative trend during 1979-1993 ($-0.05^{\circ}\text{C}/\text{decade}$) whereas a positive trend from 1994 to 2018 ($\sim+0.1^{\circ}\text{C}/\text{decade}$; Fig. 3c) indicating that more heat was lost to the atmosphere during the latter than in the former decades. This is further confirmed by a decrease in latent heat and net heat flux rates (-2.05 and $-3.25 \text{ Wm}^{-2} \text{ decade}^{-1}$) between 1994 and 2019 than 1970-1993 (10.19 and $11.07 \text{ W m}^{-2} \text{ decade}^{-1}$) during winter suggesting that evaporation increased during the former period leading to strengthening of convective mixing (Table 1; Fig. 3, S1). The specific humidity also plays a crucial role, apart from net heat flux at the surface, in the strengthening of convective mixing in the recent decades (1994-2018) in the northern AS.

4.2. Long-term trends in specific humidity and mixing of the upper ocean in the northern AS during winter

The spatial contrasting sea to atmospheric moisture was noticed between 1979 to 1993 and 1994 to 2018 (Fig. 2e-f). The flux of moisture from sea to atmosphere is dependent on humidity in the atmosphere. Dry and cool winds from the northeast of the AS can enhance moisture transport from sea to atmosphere leading to an increase in the density of surface waters that triggers convective mixing (Kumar and Prasad, 1996; Madhupratap et al., 1996). Based on the climatological data, northern AS contributes to $\sim 60\%$ of the net evaporation-precipitation (E-P) during winter to net annual evaporation of $1000 \text{ mm}/\text{y}$ (Tomczak and Godfrey, 1994). Weller et al. (1998) reported that mean relative humidity over northern AS was $\sim 70\%$ during winter favoured high evaporation leading to an increase in surface density and deepening of MLD (Wiggert et al., 2000). The mean relative humidity during the winter of 1994-2018 was $\sim 78\%$, which can trigger convective mixing in the northern AS. The difference in saturation to atmosphere-specific humidity (δq) explains the evaporation/net loss of the water from the ocean surface to the atmosphere and it was decreased at a rate of $-0.06 \text{ g}/\text{kg}/\text{decade}$ from 1979 to 1993 but increased ($+0.14 \text{ g}/\text{kg}/\text{decade}$; Fig. 2c,d and 3d) from 1994 to 2018 indicating that evaporation increased in the northern AS during the latter decades. This is consistent with the decrease in latent heat and net heat fluxes (-2.15 and $-3.2 \text{ Wm}^{-2} \text{ decade}^{-1}$, Table 1; Fig. 2g,h) and a slight decrease in surface salinity ($-0.01 /\text{decade}$; Fig. 3b) from 1994 to 2018 confirming that convective mixing enhanced in the recent decades.

The mean winter wind speed displayed decreasing trend at the rate of -0.32 and -0.003 m/s/decade during 1979-93 and 1994-2018 respectively (Table 1 & Fig. 2c-d) and it is 4 times lower than the value reported by Goes et al. (2020) due to selection of variable regions and months. The spatial variations in the trends in winds displayed significant increasing trends in southwestern AS from 1994 to 2018 whereas insignificant trends in the other regions (Fig. 2c,d). Parvathi et al. (2017) projected a weakened convective mixing at the end of the 21st century based on Coupled Model Intercomparison Project Phase 5 (CMIP5) models under RCP 8.5 and 4.5 scenarios. The reduction in the interhemispheric sea level pressure gradient weakened the winds due to the relatively higher warming of the dry Arabian Peninsula than the Southern Indian Ocean resulting in a weakening of convective mixing. The weak trends in winds during the present study are for a shorter period (1979-2018) compared to Parvathi et al. (2017) analysis, which is a projection for the end of the 21st century. Sarma et al. (2013) compared the different global model performances for pCO₂ levels and fluxes at the air-sea interface under the aegis of REgional Carbon Cycle Assessment and Processes (RECCAP) and found that none of the models is performing well in simulating the seasonal cycle of pCO₂ in the northern Indian Ocean due to poor simulation of monsoon currents and mixing. Nevertheless, the weak long-term trend in winds during the study period indicates that the contribution of winds to change in evaporation may be insignificant. Based on the trends in latent heat and net heat flux, evaporation was increased in the recent decades, but it was not significantly contributed by the winds, in the AS during the study period.

The strengthened convective mixing in the recent decades may deepen the depth of the mixed layer during winter (Fig. 3f). The spatial variations in trends in MLD did not show specific trends from 1979 to 1993 whereas the decreasing trend was noticed in the southern AS but no significant trends in the northern AS. (Table 1; Fig. S1e,f). Goes et al. (2020) reported shallowing of MLD during winter (January, February and March) at the rate of 2.8 m/decade during the period between 1980 and 2018. The shallow MLD of 20 to 30 m was reported during March/April due to strong thermal stratification (Morrison et al., 1998). Due to the addition of March data in the winter mean computations, shoaling of MLD was noticed (2.8 m/decade) by Goes et al., (2020). Considering the higher magnitude of uncertainties in MLD data, the long-term variability in the depth of 20°C (D20) isotherm is examined. The seasonal mean D20 deepened at the rate of 2-6.0m/decade (Fig. S1h) from 1994 to 2018 in the AS whereas

insignificant trends were noticed, except for a small pocket in the central AS, from 1979 to 1993 (Fig. S2g). The mean rate of deepening of D20 was 6.7 m/decade in the selected region in the northern AS (Table 1) and no significant trend was observed from 1979 to 1993 (Fig. 3e). In addition to this, the measured D20 by Argo floats data suggested that D20 shallowed at the rate of 12.6 m/decade between 2004 and 2018 and it is consistent with modelled data (17.7 m/decade) indicating that convective mixing was strengthened during recent decades (Fig. 3e).

In summary, cooling of AT due to atmospheric aerosols and cold waves and warming of SST enhanced the difference in sea-to-air temperature gradient associated with larger sea-to-air specific humidity difference (leading to increased evaporation) contributing to an increase in net heat flux to the atmosphere from the northern AS during 1994-2018. The variability in air-sea interactions strengthened the convective mixing in recent decades. This may result in enhanced input of nutrients to the photic zone through entrainment.

4.3. Trends in surface Chlorophyll-a due to variation in convective mixing in the northern AS

The variability in the surface Chl-a is mainly dependent on the availability of nutrients and mixing. The deepening of the mixed layer is an indicator of the input of nutrients to the surface layer. An increase in nitrate concentrations ($>2 \mu\text{M}$) was reported during winter in the northern AS (Madhupratap et al., 1996; Morrison et al., 1998; Prakash et al., 2017; Sarma et al., 2019). The trends in winter mean surface Chl-a varied between -0.04 and $+0.03 \text{ mg/m}^3/\text{decade}$ but they are not statistically significant (Supplementary Figure S5). The rate of increasing trends was relatively higher ($0.05 \text{ mg/m}^3/\text{decade}$) during February than in other months (Table 1; Supplementary Figure S4g). The rate of increase in Chl-a is contrasting to that of sea-air temperature difference, which was the least during February ($0.02^\circ\text{C}/\text{decade}$) compared to that in December ($0.15^\circ\text{C}/\text{decade}$) and January ($0.11^\circ\text{C}/\text{decade}$) indicating the weaker mixing in February led to increasing the stability of water column and formation of *Noctiluca* blooms (Xiang et al., 2019; Table 1; Fig. S2-4). Sarma et al. (2019) reported that *Noctiluca scintillans* blooms occur in the middle of February associated with shallowing of the mixed layer due to westward advection of coastal waters and low silicate concentrations (Prakash et al., 2017; Xiang et al., 2019). Though *Noctiluca* does not require nutrients, diatoms are their preferred prey for them hence they mostly develop following diatom blooms (Kiorboe and Titelman, 1998; Dwivedi et al., 2015; Gomes et al., 2018). Therefore, enhanced convective mixing increased the

availability of nutrients, including silicate, that lead to the enhanced abundance of diatom in recent decades, which acted as prey for *Noctiluca* resulting in enhanced *Noctiluca* blooms. In addition to this, anthropogenic aerosols bring a significant amount of nitrogen and iron to the northern AS during winter and support phytoplankton biomass. Guieu et al. (2019) estimated that atmospheric deposition of nitrogen and iron enhances primary production by 22% during winter. The rate of anthropogenic AOD was noticed during winter (Fig. 5 and Table 1) indicating that more nutrient deposition is possible from the atmosphere resulting in an increase in phytoplankton biomass in the recent decades. Therefore, the increase in phytoplankton biomass in the recent decades may be contributed by both strengthening of convective mixing and deposition of nutrients from the atmospheric dry deposition in the northern AS that supported enhanced *Noctiluca scintillans* blooms in the northern AS.

The enhanced phytoplankton biomass in recent decades may enhance the sinking of carbon fluxes to subsurface layers, which may lead to the intensification of OMZ. Banse et al. (2014) reported depletion of oxygen in the OMZ by 0.19 $\mu\text{M}/\text{y}$ during winter from 1959 to 2004 between 15 and 20°N and it is consistent with an increase in Chl-a in the recent decades (Table 1). Therefore, this study strongly points out that winter convective mixing has strengthened due to a decrease in AT caused by an increase in atmospheric aerosols and cold waves increasing phytoplankton blooms, leading to the formation of mixotrophic *Noctiluca scintillans* in the northern AS.

Summary and Conclusions

Long-term variability over 4 decades (1979-2018) suggests that significant cooling of AT was observed during winter between 1994 and 2018 whereas significant warming was noticed during 1979-1993 associated with a significant increase in atmospheric aerosols in the former period due to rapid industrialization in the South and Southeast Asia. In contrast, SST was warmed during the entire study period (1979-2018, except in February) with relatively higher warming during 1979-1993 than 1994-2018 but the warming/cooling rates are not statistically significant during 1994-2018. The difference between SST to AT decreased from 1979-to 1993 but increased from 1994-to 2018. Based on the increase in the difference between SST and AT, specific humidity difference (δq), net surface heat flux loss, and trends in latent heat flux associated with the deepening of D20, it is clear that winter convective mixing strengthened in

the recent decades (1994-2018) than it was hitherto hypothesized as weakened due to reduction in snow cover over the Eurasian land. The deepening of D20, under the influence of convective mixing, enhanced nutrient concentrations into the euphotic zone increasing phytoplankton biomass, mainly diatoms. In addition to the increased nutrient input due to the strengthening of convective mixing, the dry depositional flux of nutrients (nitrogen and iron) from atmospheric aerosols also contributed to an increase in phytoplankton blooms that result in the enhanced intensity of *Noctiluca sintillans* blooms in the northern AS in the recent decades.

Acknowledgements:

We would like to thank the National Ocean and Atmospheric Administration (NOAA) for making available long-term data on SST, AT and Global Ocean Assimilation System (GODAS) for Mixed Layer Depth, SeaWiFS and MODIS Chl-a, AOD, and NCEP for winds data. We would like to thank two anonymous reviewers for their critical review to improve the presentation of this manuscript. The data used in this study are freely available to the public and the source website information is given in the data and methodology section. This has NIO contribution number xxxxxx

References

- Andreae, M.O. and Rosenfeld, D.J.E.S.R., 2008. Aerosol–cloud–precipitation interactions. Part 1. The nature and sources of cloud-active aerosols. *Earth-Science Reviews*, 89(1-2), pp.13-41.
- Baek, S.H., Shimode, S., Kim, H.C., Han, M.S. and Kikuchi, T., 2009. Strong bottom–up effects on phytoplankton community caused by a rainfall during spring and summer in Sagami Bay, Japan. *Journal of Marine Systems*, 75(1-2), pp.253-264.
- Banse, K., Naqvi, S.W.A., Narvekar, P.V., Postel, J.R. and Jayakumar, D.A. 2014. Oxygen minimum zone of the open Arabian Sea: variability of oxygen and nitrite from daily to decadal time scales. *Biogeosciences*, 11, 2237-2261.
- Barber, R.T., Marra, J., Bidigare, R.C., Codispoti, L.A., Halpern, D., Johnson, Z., Latasa, M., Goericke, R. and Smith, S.L., 2001. Primary productivity and its regulation in the Arabian Sea during 1995. *Deep Sea Res., Part II, Topical Studies in Oceanography*, 48(6-7), pp.1127-1172.
- Bhattathiri, P.M.A., Pant, A., Sawant, S., Gauns, M., Matondkar, S.G.P. and Mohanraju, R., 1996. Phytoplankton production and chlorophyll. *Curr. Sci.*, 71(11).
- Boucher, Olivier, David Randall, Paulo Artaxo, Christopher Bretherton, Gragam Feingold, Piers Forster, V. M. Kerminen et al. "Clouds and aerosols. Climate change 2013: The physical science basis. Contribution of working group I to the fifth assessment report of the intergovernmental panel on climate change." Cambridge University Press, Cambridge, United Kingdom and New York, NY, USA (2013): 571-657.
- Buesseler, K.O., Ball, L., Andrews, J., Belostock, R. and Benitez-Nelson, C., 1996. Upper ocean particulate export in the Arabian Sea. *EOS*, 77(46), p.F96.
- Cold Waves, 2018. *Weather N Climate*. Vol. 12, Issue 75.
- De Sousa, S.N., Kumar, M.D., Sardesai, S. and Sarma, V.V.S.S., 1996. Seasonal variability in oxygen and nutrients in. *Curr. Sci.*, 71(11).
- Dickey, T., Marra, J., Sigurdson, D.E., Weller, R.A., Kinkade, C.S., Zedler, S.E., Wiggert, J.D. and Langdon, C., 1998. Seasonal variability of bio-optical and physical properties in the Arabian Sea: October 1994-October 1995. *Deep Sea Res., Part II, Topical studies in Oceanography*, 45(10-11), pp.2001-2025.
- Dimri, A.P., Niyogi, D., Barros, A.P., Ridley, J., Mohanty, U.C., Yasunari, T. and Sikka, D.R., 2015. Western disturbances: a review. *Rev. of Geophys.*, 53(2), pp.225-246.
- Dong, Lu., and Tianjun, Zhou., 2014. The Indian Ocean Sea Surface Temperature Warming Simulated by CMIP5 Models during the Twentieth Century: Competing Forcing Roles of GHGs and Anthropogenic Aerosols. *J. Clim.* 27(9), <https://doi.org/10.1175/JCLI-D-13-00396.1>

Dwivedi, R.M., Raman, M., Parab, S., Matondkar, S.G.P. and Nayak, S., 2006. Influence of northeasterly trade winds on intensity of winter bloom in the Northern Arabian Sea. *Current Science*, pp.1397-1406.

Dwivedi, R., Rafeeq, M., Smitha, B.R., Padmakumar, K.B., Thomas, L.C., Sanjeevan, V.N., Prakash, P. and Raman, M., 2015. Species identification of mixed algal bloom in the Northern Arabian Sea using remote sensing techniques. *Environmental monitoring and assessment*, 187(2), pp.1-11.

Goes, J.I., Thoppil, P.G., do R Gomes, H. and Fasullo, J.T., 2005. Warming of the Eurasian landmass is making the Arabian Sea more productive. *Science*, 308(5721), pp.545-547.

Goes, J.I., Tian, H., do Rosario Gomes, H., Anderson, O.R., Al-Hashmi, K., deRada, S., Luo, H., Al-Kharusi, L., Al-Azri, A. and Martinson, D.G., 2020. Ecosystem state change in the Arabian Sea fuelled by the recent loss of snow over the Himalayan-tibetan plateau region. *Scientific Reports*, 10(1), pp.1-8.

Gomes, do Rosario H., Goes, J.I., Matondkar, S.P., Parab, S.G., Al-Azri, A.R. and Thoppil, P.G., 2008. Blooms of *Noctiluca miliaris* in the Arabian Sea—An in situ and satellite study. *Deep Sea Research Part I: Oceanographic Research Papers*, 55(6), pp.751-765.

Gomes, H. do Rosário, Goes, J.I., Matondkar, S.P., Buskey, E.J., Basu, S., Parab, S. and Thoppil, P., 2014. Massive outbreaks of *Noctiluca scintillans* blooms in the Arabian Sea due to spread of hypoxia. *Nature Communications*, 5(1), pp.1-8.

Gomes, H.D.R., McKee, K., Mile, A., Thandapu, S., Al-Hashmi, K., Jiang, X. and Goes, J.I., 2018. Influence of light availability and prey type on the growth and photo-physiological rates of the mixotroph *Noctiluca scintillans*. *Frontiers in Marine Science*, 5, p.374.

Guieu, C., Al Azhar, M., Aumont, O., Mahowald, N., Levy, M., Ethe, C., and Lachkar, Z. 2019. Major impact of dust deposition on the productivity of the Arabian Sea. *Geophys. Res. Lett.*, 46, 7636-6744.

Harrison, P.J., Furuya, K., Glibert, P.M., Xu, J., Liu, H.B., Yin, K., Lee, J.H., Anderson, D.M., Gowen, R., Al-Azri, A.R. and Ho, A.Y.T., 2011. Geographical distribution of red and green *Noctiluca scintillans*. *Chinese Journal of Oceanology and Limnology*, 29(4), pp.807-831.

Hastenrath, S. and Lamb, P.J., 1979. *Climatic Atlas of the Indian Ocean*, vol. 1, Surface Climate and Atmospheric Circulation. University of Wisconsin Press, 1, p.16.

IPCC (Intergovernmental Panel on Climate Change). 2001. The observed changes in the climate system. In: *Climate Change 2001: The Scientific Basis* (eds. J. T. Houghton, Y. Ding, D. J. Griggs, M. Noguer, P. J. van der Linden and co-authors). Cambridge University Press, New York, pp. 25-30.

- IPCC, 2013, Summary for Policymakers. In: Climate Change 2013: The Physical Science Basis. Contribution of Working Group I to the Fifth Assessment Report of the Intergovernmental Panel on Climate Change (Stocker, T.F., D. Qin, G.-K. Plattner, M. Tignor, S.K. Allen, J. Boschung, A. Nauels, Y. Xia, V. Bex and P.M. Midgley (eds.)). Cambridge University Press, Cambridge, United Kingdom and New York, NY, USA.
- Kaufman, Y.J., Boucher, O., Tanré, D., Chin, M., Remer, L.A., and Takemura, T., 2005a. Aerosol anthropogenic component estimated from satellite data. *Geophys. Res. Lett.*, 32(17)
- Kaufman, Y.J., Koren, I., Remer, L.A., Tanré, D., Ginoux, P. and Fan, S., 2005b. Dust transport and deposition observed from the Terra-Moderate Resolution Imaging Spectroradiometer (MODIS) spacecraft over the Atlantic Ocean. *Journal of Geophysical Research: Atmospheres*, 110(D10).
- Kjørboe, T. and Titelman, J., 1998. Feeding, prey selection and prey encounter mechanisms in the heterotrophic dinoflagellate *Noctiluca scintillans*. *Journal of Plankton Research*, 20(8), pp.1615-1636.
- Kothawale, D.R. and Kumar, K.R., 2002. Tropospheric temperature variation over India and links with the Indian summer monsoon: 1971-2000. *Mausam*, 53(3), pp.289-308.
- Krishna Moorthy, K., Suresh Babu, S., Manoj, M.R., Satheesh, S.K., 2013. Buildup of aerosols over the Indian Region. *Geophys. Res. Lett.* 40:1011–1014. <https://doi.org/10.1002/grl.50165>
- Kumar, S.P. and Prasad, T.G., 1996. Winter cooling in the northern Arabian Sea. *Curr.Sci.*, pp.834-841.
- Kumar, S.P., Ramaiah, N., Gauns, M., Sarma, V.V.S.S., Muraleedharan, P.M., Raghukumar, S., Kumar, M.D. and Madhupratap, M., 2001. Physical forcing of biological productivity in the Northern Arabian Sea during the Northeast Monsoon. *Deep Sea Res., Part II, Topical Studies in Oceanography*, 48(6-7), pp.1115-1126.
- Kumar, P.D., Paul, Y.S., Muraleedharan, K.R., Murty, V.S.N. and Preenu, P.N., 2016. Comparison of long-term variability of Sea Surface Temperature in the Arabian Sea and Bay of Bengal. *Reg Stud in Mar. Sci.*, 3, pp.67-75.
- Kurokawa, J. and Ohara, T. 2020. Long-term historical trends in air pollutant emissions in Asia: Regional Emission inventory in Asia (REAS) version 3. *Atmos. Chem. Phys.*, 20, 12761-12793.
- Lotliker, A.A., Baliarsingh, S.K., Trainer, V.L., Wells, M.L., Wilson, C., Bhaskar, T.U., Samanta, A. and Shahimol, S.R., 2018. Characterization of oceanic *Noctiluca* blooms not associated with hypoxia in the Northeastern Arabian Sea. *Harmful Algae*, 74, pp.46-57.
- Madhupratap M, Kumar SP, Bhattathiri PM, Kumar MD, Raghukumar S, Nair KK, Ramaiah N. Mechanism of the biological response to winter cooling in the northeastern Arabian Sea. *Nature*, 1996 Dec;384(6609):549-52.

- Miyaguchi, H., Fujiki, T., Kikuchi, T., Kuwahara, V.S. and Toda, T., 2006. Relationship between the bloom of *Noctiluca scintillans* and environmental factors in the coastal waters of Sagami Bay, Japan. *Journal of Plankton Research*, 28(3), pp.313-324.
- Morrison, J.M., Codispoti, L.A., Gaurin, S., Jones, B., Manghnani, V. and Zheng, Z., 1998. Seasonal variation of hydrographic and nutrient fields during the US JGOFS Arabian Sea Process Study. *Deep Sea Res., Part II, Topical Studies in Oceanography*, 45(10-11), pp.2053-2101.
- Naqvi, S.W.A., Sarma, V.V.S.S. and Jayakumar, D.A., 2002. Carbon cycling in the northern Arabian Sea during the northeast monsoon: Significance of salps. *Mar Ecol Prog Ser.*, 226, pp.35-44.
- Pai, D.S., Srivastava, A.K. and Nair, S.A., 2017. Heat and cold waves over India. In *Observed climate variability and change over the Indian Region* (pp. 51-71). Springer, Singapore. DOI 10.1007/978-981-10-2531-0_4
- Parvathi, V., Suresh, I., Lengaigne, M., Izumo, T. and Vialard, J., 2017. Robust projected weakening of winter monsoon winds over the Arabian Sea under climate change. *Geophysical Research Letters*, 44(19), pp.9833-9843.
- Prakash, P., Prakash, S., Rahaman, H., Ravichandran, M. and Nayak, S., 2012. Is the trend in chlorophyll-a in the Arabian Sea decreasing?. *Geophys. Res. Lett.*, 39(23).
- Prakash, S., Roy, R. and Lotliker, A., 2017. Revisiting the *Noctiluca scintillans* paradox in northern Arabian Sea. *Curr Sci.*, 113, 1429-1434.
- Ramanathan, V., 1996. Indian Ocean Experiment (INDOEX): A Multi-agency Proposal for a Field Experiment in the Indian Ocean.
- Ramanathan, V., Crutzen, P.J., Lelieveld, J., Mitra, A.P., Althausen, D., Anderson, J., Andreae, M.O., Cantrell, W., Cass, G.R., Chung, C.E. and Clarke, A.D., 2001. Indian Ocean Experiment: An integrated analysis of the climate forcing and effects of the great Indo-Asian haze. *Journal of Geophysical Research: Atmospheres*, 106(D22), pp.28371-28398.
- Ramanathan, V., Crutzen, P.J., Mitra, A.P. and Sikka, D., 2002. The Indian Ocean experiment and the Asian brown cloud. *Current Science*, 83(8), pp.947-955.
- Ratnam, J.V., Behera, S.K., Annamalai, H., Ratna, S.B., Rajeevan, M. and Yamagata, T., 2016. ENSO's far reaching connection to Indian cold waves. *Sci. Reports*, 6(1), pp.1-12.
- Rastogi, N., Agnihotri, R., Sawlani, R., Patel, A., Babu, S.S., and Satish, R., 2020. Chemical and isotopic characteristics of PM10 over the Bay of Bengal: Effects of continental outflow on a marine environment. *Science of The Total Environment*, p.138438
- Sabine, C.L., Wanninkhof, R., Key, R.M., Goyet, C. and Millero, F.J., 2000. Seasonal CO2 fluxes in the tropical and subtropical Indian Ocean. *Mar Chem.*, 72(1), pp.33-53.

- Sarin, T.S., Vinoj, V., Swain, D., Landu, K. and Suhas, E., 2021. Aerosol induced changes in sea surface temperature over the Bay of Bengal due to COVID-19 lockdown. *Frontiers in Marine Science*, 8.
- Sarma, V.V.S.S., Kumar, M.D. and George, M.D., 1998. The central and eastern Arabian Sea as a perennial source of atmospheric carbon dioxide. *Tellus B: Chemical and Physical Meteorology*, 50(2), pp.179-184.
- Sarma, V.V.S.S., Lenton, A., Law, R.M., Metzl, N., Patra, P.K., Doney, S., Lima, I.D., Dlugokencky, E., Ramonet, M. and Valsala, V., 2013. Sea-air CO₂ fluxes in the Indian Ocean between 1990 and 2009. *Biogeosciences*, 10(11), pp.7035-7052.
- Sarma, V.V.S.S., Patil, J.S., Shankar, D. and Anil, A.C., 2019. Shallow convective mixing promotes massive *Noctiluca scintillans* bloom in the northeastern Arabian Sea. *Mar. Pollut. Bull.*, 138, 428-436.
- Sawant, S.S. and Madhupratap, M., 1996. Seasonality and composition of phytoplankton in the Arabian Sea. *Curr. Sci.*, 71, 869-873.
- Schott, F.A. and McCreary Jr, J.P., 2001. The monsoon circulation of the Indian Ocean. *Progr. Oceanogra.*, 51, 1-123.
- Srivastava, R., 2017. Trends in aerosol optical properties over South Asia. *Int J Climatol* 37:371–380. <https://doi.org/10.1002/joc.4710>
- Tomczak, M., Godfrey, J.S., 1994. *Regional Oceanography: an Introduction*. Pergamon, London, 422pp.
- Twomey, S., 1977. The influence of pollution on the shortwave albedo of clouds. *Journal of the atmospheric sciences*, 34(7), pp.1149-1152.
- Wasmund, N., Nausch, G. and Feistel, R., 2013. Silicate consumption: an indicator for long-term trends in spring diatom development in the Baltic Sea. *Journal of Plankton Research*, 35(2), pp.393-406.
- Weller, R.A., Baumgartner, M.F., Josey, S.A., Fischer, A.S. and Kindle, J.C., 1998. Atmospheric forcing in the Arabian Sea during 1994–1995: Observations and comparisons with climatology and models. *Deep Sea Res., Part II: Topical Studies in Oceanography*, 45(10-11), pp.1961-1999.
- Wei, J., Peng, Y., Mahmood, R., Sun, L. and Guo, J., 2019. Intercomparison in spatial distributions and temporal trends derived from multi-source satellite aerosol products. *Atmospheric Chemistry and Physics*, 19(10), pp.7183-7207.
- Wiggert, J.D., Jones, B.H., Dickey, T.D., Brink, K.H., Weller, R.A., Marra, J. and Codispoti, L.A., 2000. The Northeast Monsoon's impact on mixing, phytoplankton biomass and nutrient cycling in the Arabian Sea. *Deep Sea Res., Part II: Topical Studies in Oceanography*, 47(7-8), 1353-1385.

Xiang, C., Tan, Y., Zhang, H., Liu, J., Ke, Z. and Li, G., 2019. The key to dinoflagellate (*Noctiluca scintillans*) blooming and outcompeting diatoms in winter off Pakistan, northern Arabian Sea. *Science of The Total Environment*, 694, p.133396.

Yadav, K., Rao, V.D., Sridevi, B. and Sarma, V.V.S.S., 2021. Decadal variations in natural and anthropogenic aerosol optical depth over the Bay of Bengal: the influence of pollutants from Indo-Gangetic Plain. *Environmental Science and Pollution Research*, 28(39), pp.55202-55219.

Yu, H., Kaufman, Y.J., Chin, M., Feingold, G., Remer, L.A., Anderson, T.L., Balkanski, Y., Bellouin, N., Boucher, O., Christopher, S. and DeCola, P., 2006. A review of measurement-based assessments of the aerosol direct radiative effect and forcing. *Atmospheric Chemistry and Physics*, 6(3), pp.613-666.

Yu, Lisan., 2003. Variability of the depth of the 20°C isotherm along 6°N in the Bay of Bengal: its response to remote and local forcing and its relation to satellite SSH variability. *Deep Sea Res., Part II: Topical Studies in Oceanography*, 50(12–13).

Zhang, J., and Reid, J.S., 2010. A decadal regional and global trend analysis of the aerosol optical depth using a data-assimilation grade over-water MODIS and Level 2 MISR aerosol products. North Dakota Univ Grand Forks Dept Of Atmospheric Sciences.

Zhao, T.X.P., Laszlo, I., Guo, W., Heidinger, A., Cao, C., Jelenak, A., Tarpley, D., and Sullivan, J., 2008, Study of long-term trend in aerosol optical thickness observed from operational AVHRR satellite instrument. *J. Geophys. Res. Lett.*, *Atmospheres*, 113(D7)

Table 1: The rate of decadal variability in different physical, meteorological and phytoplankton biomass properties in the northern Arabian Sea (18-22°N and 62-68°E) for December, January and February and winter season (DJF) for each of two different decadal periods during (1979-2018). Slopes are in per decade. ****, ***, **, * represents $p < 0.001, 0.01, 0.05, 0.1$ respectively

Parameter	Period	Slope per decade			
		Dec	Jan	Feb	DJF
AT (°C)	1979-1993	0.661**	0.520**	0.690*	0.587**
	1994-2018	-0.060	-0.081	-0.046	-0.054
SST (°C)	1979-1993	0.411*	0.523**	0.691**	0.535**
	1994-2018	0.092	0.024	-0.027	0.043
δT (°C)	1979-1993	-0.251**	0.003	0.001	-0.052
	1994-2018	0.152*	0.105*	0.019	0.098*
D20 (m)	1979-1993	-1.298	4.186	4.831	-1.242
	1994-2018	6.397***	5.928***	5.699***	6.676***
Salinity (psu)	1979-1993	-0.088*	-0.053	-0.070*	-0.088**
	1994-2018	0.003	-0.012	-0.015	-0.009
Wind (m/s)	1979-1993	-0.190	-0.202	-0.150	-0.315
	1994-2018	0.045	-0.190	0.171	-0.003
Qa (g/kg)	1979-1993	0.939**	0.876*	0.627	0.708*
	1994-2018	-0.189	-0.067	-0.037	-0.082
dq (g/kg)	1979-1993	-0.422	-0.253	0.183	-0.062
	1994-2018	0.319	0.094	0.004	0.141
LHF (w/m ²)	1979-1993	17.18	12.15	0.49	10.19
	1994-2018	-9.7	5.02	-3.46	-2.05
Net Heat Flux (W/m ²)	1979-1993	16.456	17.692	1.475	11.079
	1994-2018	-9.631	5.759	-7.165	-3.247
MLD (m) (GODAS)	1979-1993	-5.127*	-6.031	-7.818	-7.848***
	1994-2018	-0.868	-0.613	-0.453	-1.093
MLD (m) (CMEMS)	1994-2018	1.14	1.12	1.82	1.15
Chl-a (mg/m ³)	2001-2018	-0.028	-0.0008	0.046	-0.046

Legend to figures

Figure 1: Spatial variations of mean winter season (DJF, 2001-2019) a) SST ($^{\circ}\text{C}$), b) GODAS-MLD (m), c) concentration of Chl-a (mg/m^3) and d) AOD in the Arabian Sea. The black box region denotes the region considered for time-series analysis.

Figure 2: Long-term spatial trends (per decade) of difference of SST and Air temperature (a, b), wind (c, d), the difference of sea to air specific humidity (e, f), and latent heat flux (g, h) between 1979 and 1993 (left panel) and between 1994 and 2018 (right panel). The solid black line represents the value of p is 0.1.

Figure 3: Long term mean trends of (a) Air Temperature (AT, $^{\circ}\text{C}$), (b) Sea Surface Temperature (SST, $^{\circ}\text{C}$, left axis), and Sea Surface Salinity (SSS, right axis; red in color) (c) Temperature difference between SST and AT (δT , $^{\circ}\text{C}$), (d) Specific humidity difference at sea surface and air (δq , g/kg), (e) D20 (m), (f) MLD (left axis for GODAS (black in color) and right axis for CMEMS (red in color), and (g) Chlorophyll-a in the selected region in Figure 1 during winter. Note: slopes given per decade and ***, **, * represents $p < 0.01, 0.05, 0.1$ respectively

Figure 4: Monthly Seasonal mean rate of increase (positive) or decrease (negative) of Total AOD overlaid with wind vectors during the period 2001-2019. The box in the figure represents the present study area.

Figure 5: Monthly Seasonal mean rate of increase (positive) or decrease (negative) of Anthropogenic AOD during the period 2001-2019. The thick black line represents a 90% significant line. The box in the figure represents the present study area.

Figure 6: Linear trends of Total (a-d) and Anthropogenic AOD (e-h) in the months of December, January, February and winter seasonal mean (DJF). Corresponding slopes and p-values are given for each trendline.

Figure 1: Spatial variations of mean winter season (DJF, 2001-2019) a) SST ($^{\circ}\text{C}$), b) GODAS-MLD (m), c) concentration of Chl-a (mg/m^3) and d) AOD in the Arabian Sea. The black box region denotes the region considered for time-series analysis.

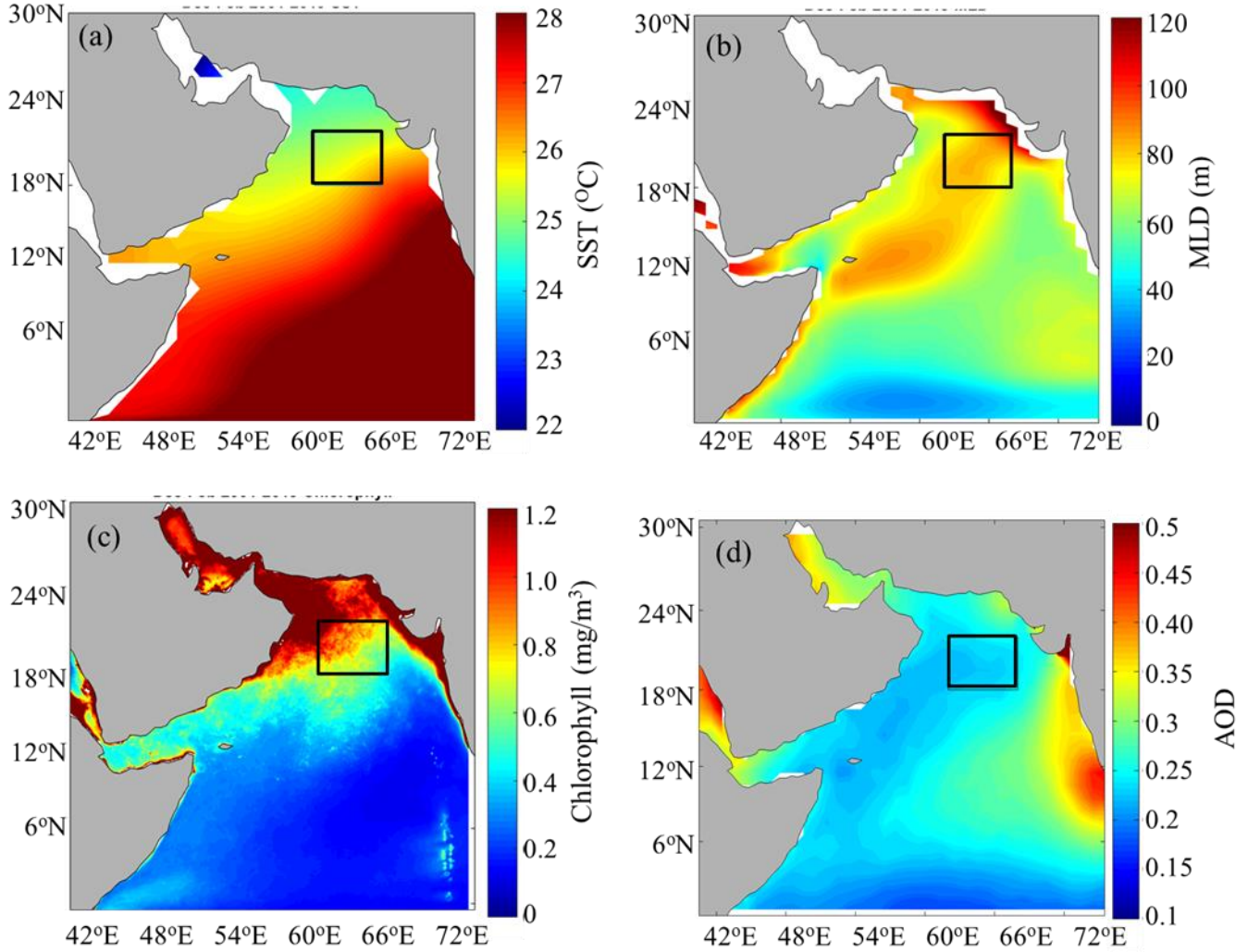


Figure 2: Long term spatial trends (per decade) of difference of SST and Air temperature (a, b), wind (c, d), difference of sea to air specific humidity (e, f), and latent heat flux (g, h) between 1979 and 1993 (left panel) and between 1994 and 2018 (right panel). The solid black line represents the value of p is 0.1.

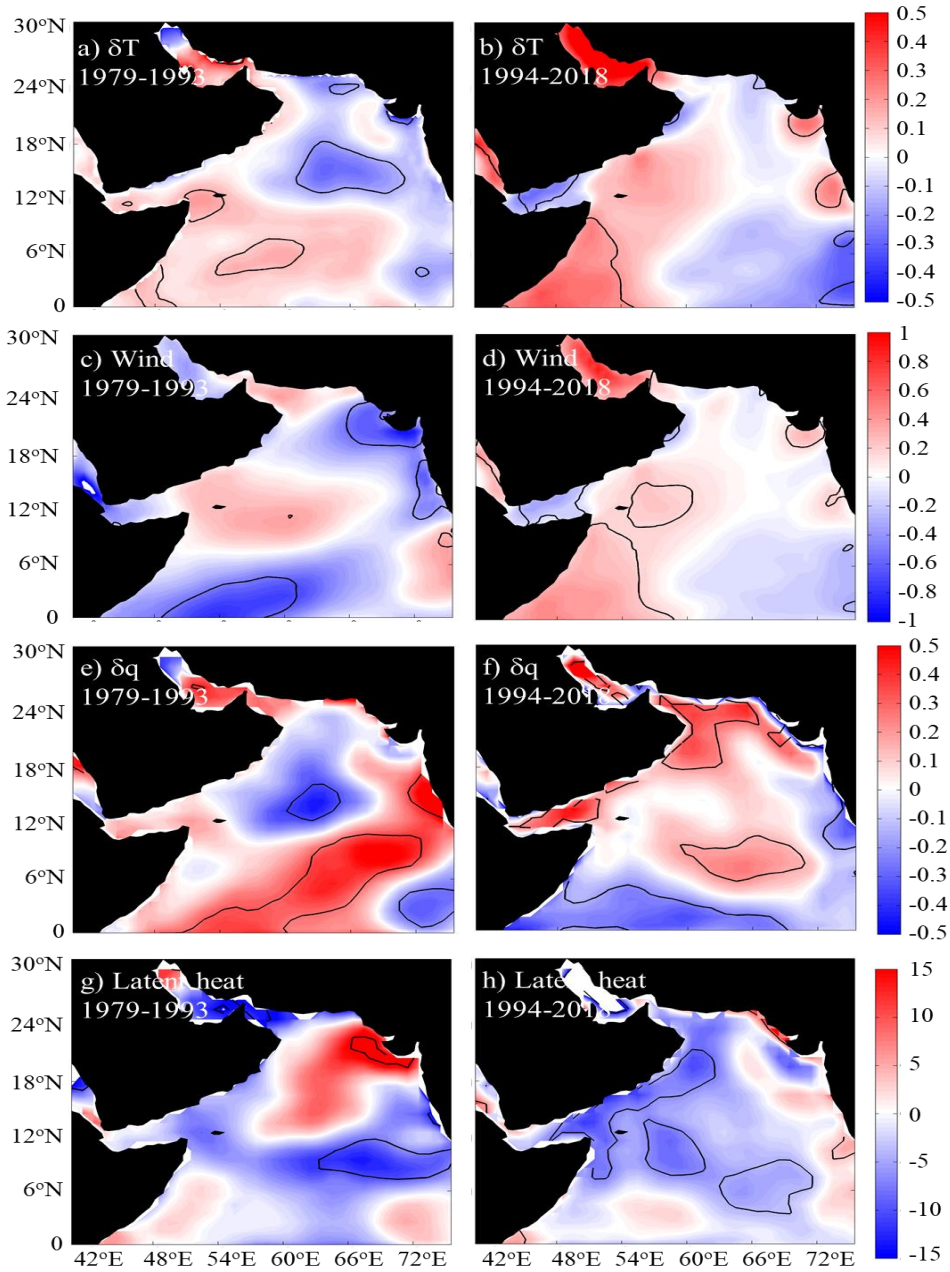


Figure 3: Long term mean trends of (a) Air Temperature (AT, °C), (b) Sea Surface Temperature (SST, °C, left axis), and Sea Surface Salinity (SSS, right axis; red in color) (c) Temperature difference between SST and AT (δT , °C), (d) Specific humidity difference at sea surface and air (δq , g/kg), (e) D20 (m), (f) MLD (left axis for GODAS (black in color) and right axis for CMEMS (red in color)), and (g) Chlorophyll-a in the selected region in Figure 1 during winter. Note: slopes given per decade and ***, **, * represents $p < 0.01, 0.05, 0.1$ respectively

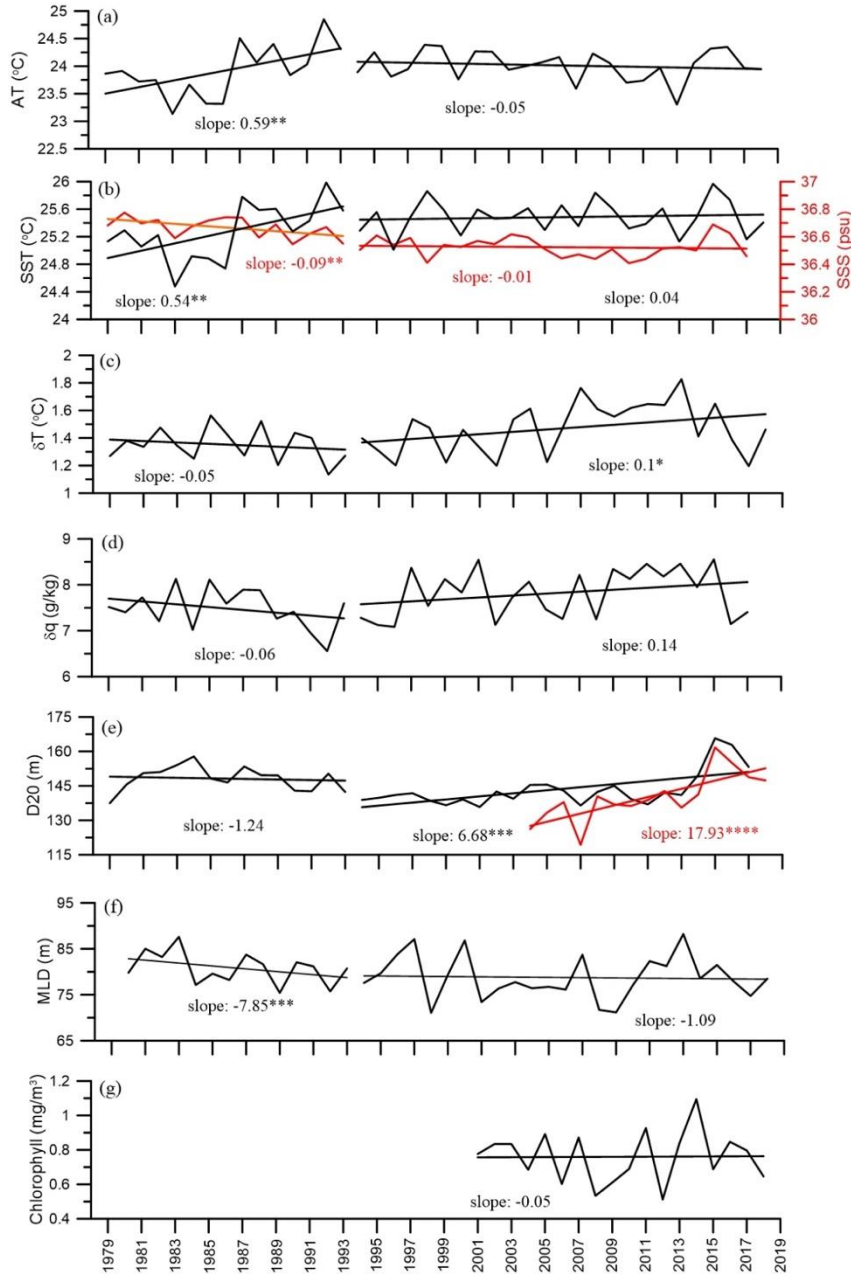


Figure 4: Monthly Seasonal mean rate of increase (positive) or decrease (negative) of Total AOD overlaid with wind vectors during the period 2001-2019. Box in the figure represents present study area.

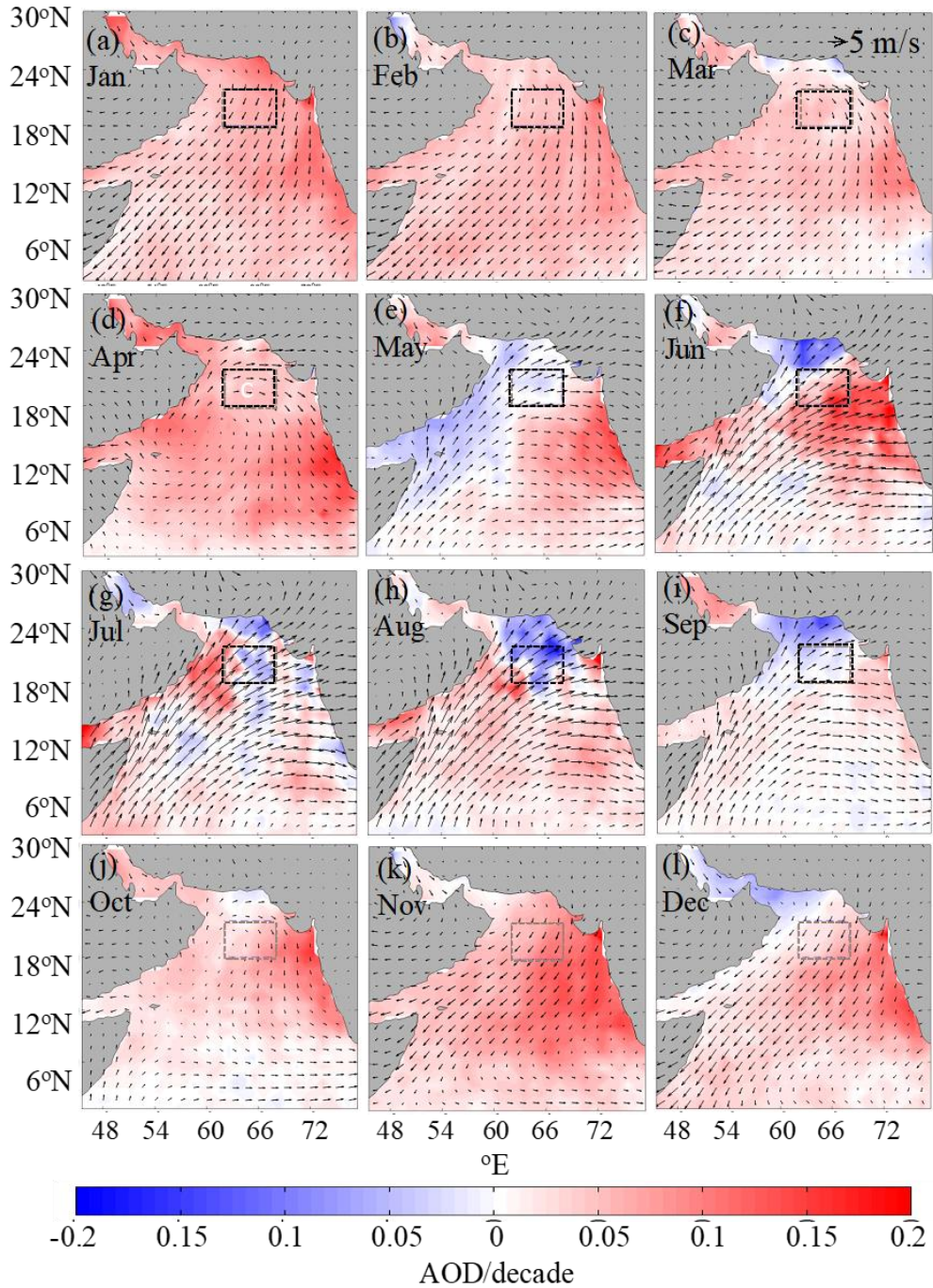


Figure 5: Monthly Seasonal mean rate of increase (positive) or decrease (negative) of Anthropogenic AOD during the period 2001-2019. Thick black line represents 90% significant line. Box in the figure represents present study area.

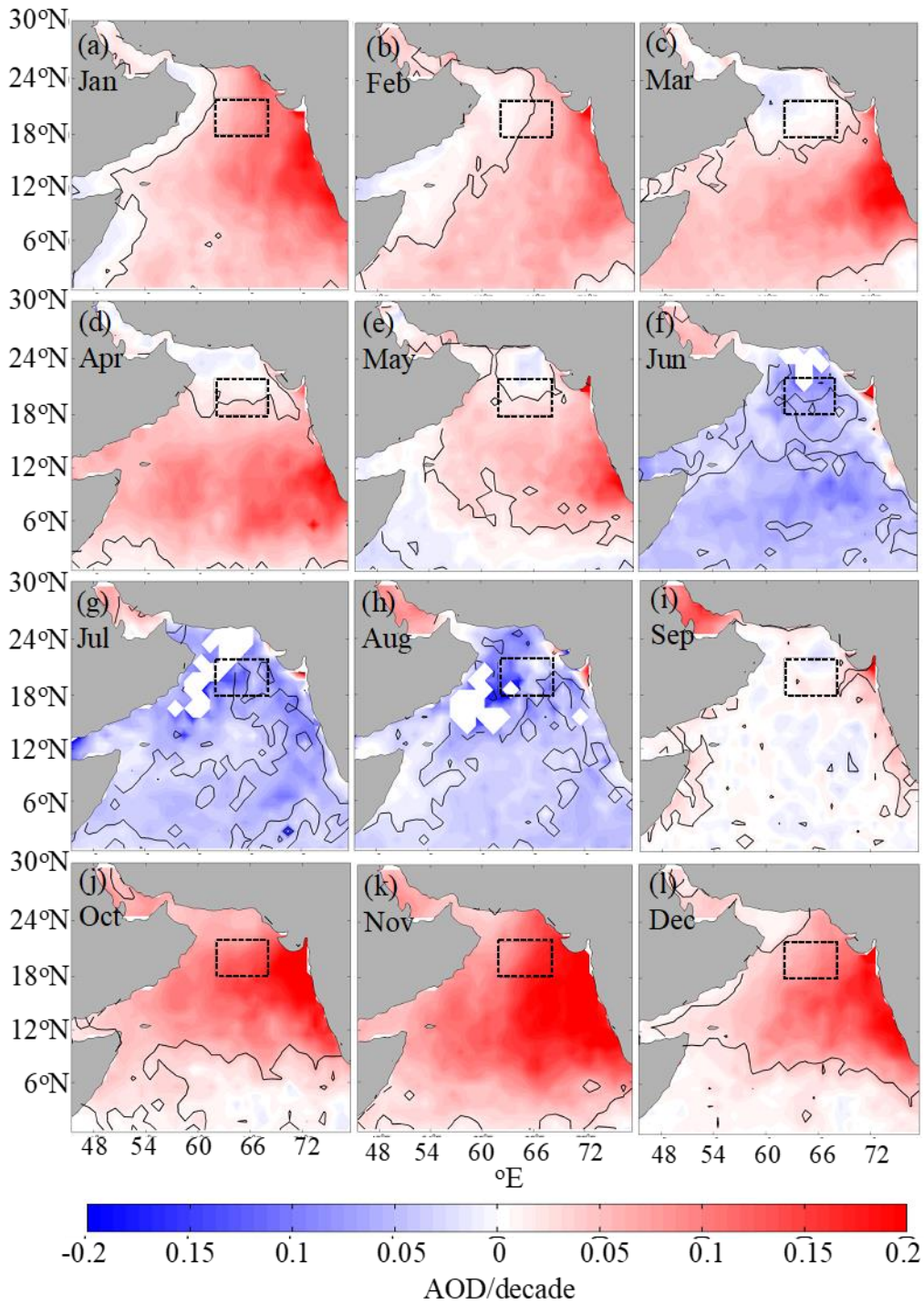
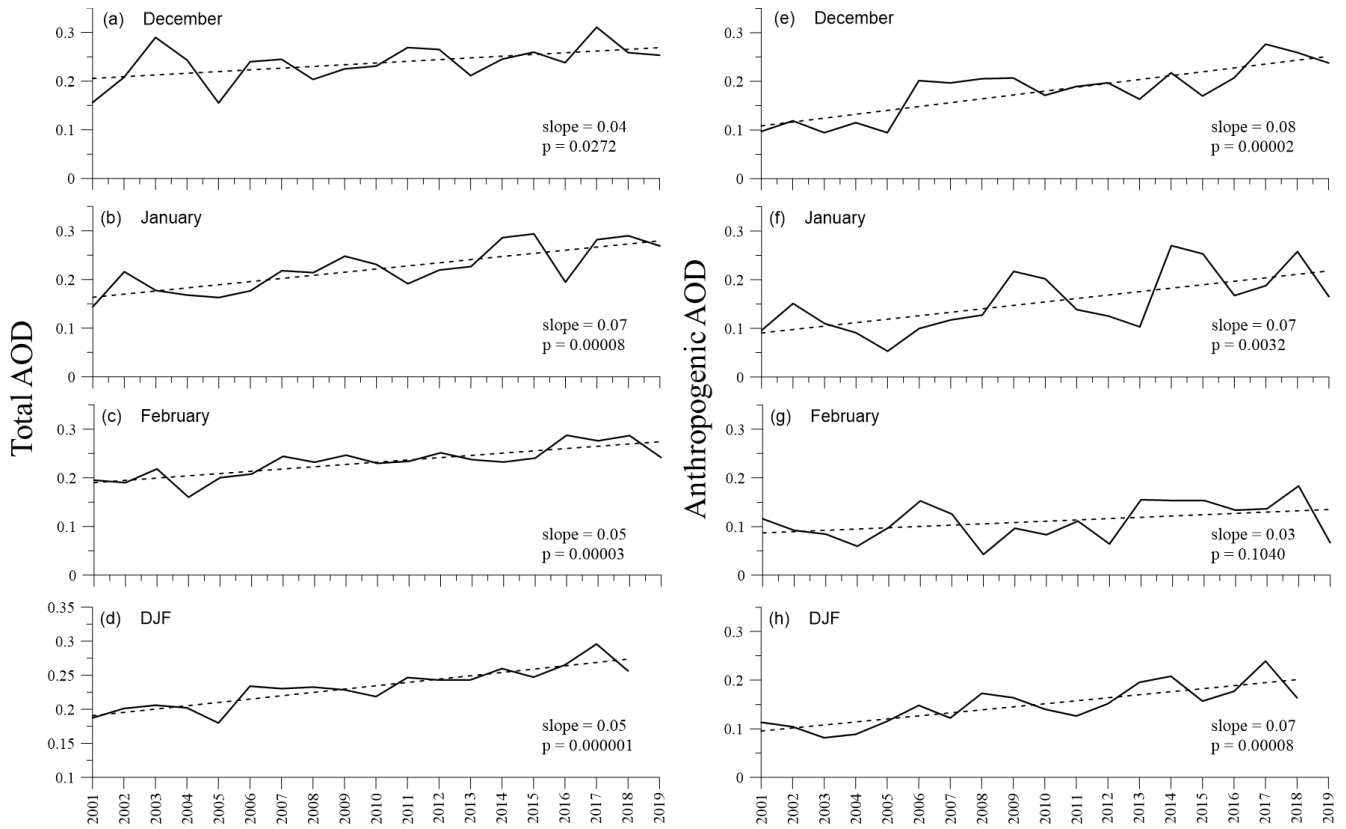


Figure 6: Linear trends of Total (a-d) and Anthropogenic AOD (e-h) in the months of December, January, February and winter seasonal mean (DJF). Corresponding slopes and p-values are given for each trendline.



Supplementary Figures:

Figure S1: Long term spatial trends (per decade) of Air temperature (a, b), SST (c, d), MLD (e, f), D20 (g, h) and net heat flux (i, j) between 1979 and 1993 (left panel) and between 1994 and 2018 (right panel). The solid black line represents the value of p is 0.1.

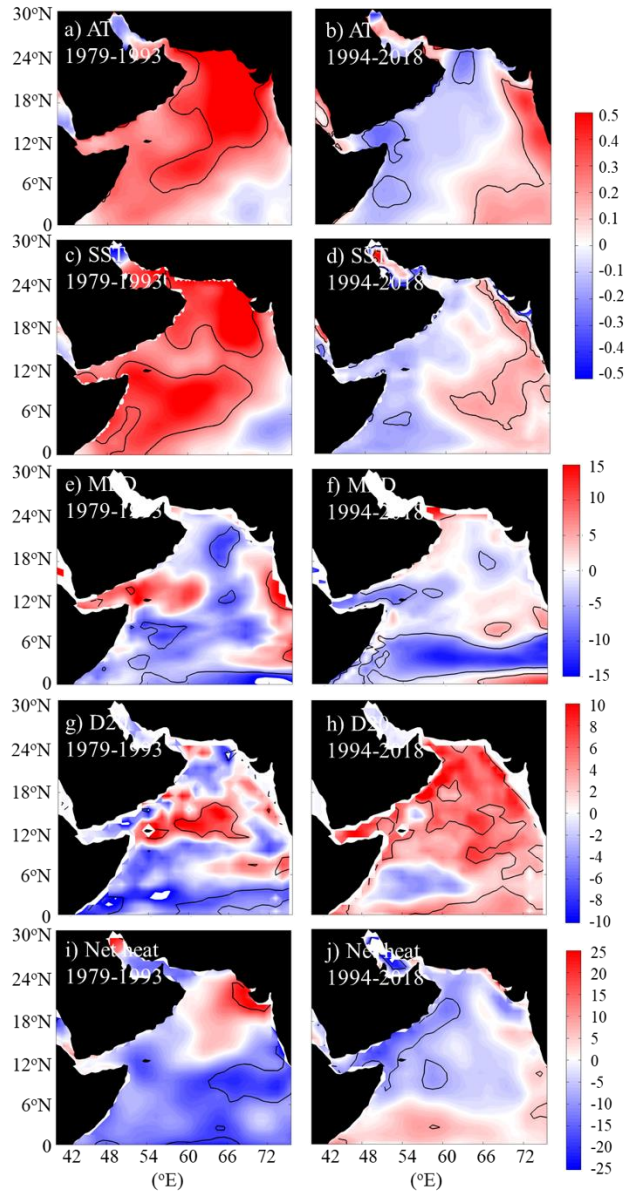


Figure S2: Long term trends of (a) Air Temperature (AT, °C), (b) Sea Surface Temperature (SST, °C, left axis), and Sea Surface Salinity (SSS, right axis; red in color) (c) Temperature difference between SST and AT (δT , °C), (d) Specific humidity difference at sea surface and air (δq , g/kg), (e) D20 (m) from ORAS5 (black in color) and Argo (red in color), (f) MLD (g) Chlorophyll-a in the month of December. Note: slopes given per decade and ***, **, * represents $p < 0.01, 0.05, 0.1$ respectively

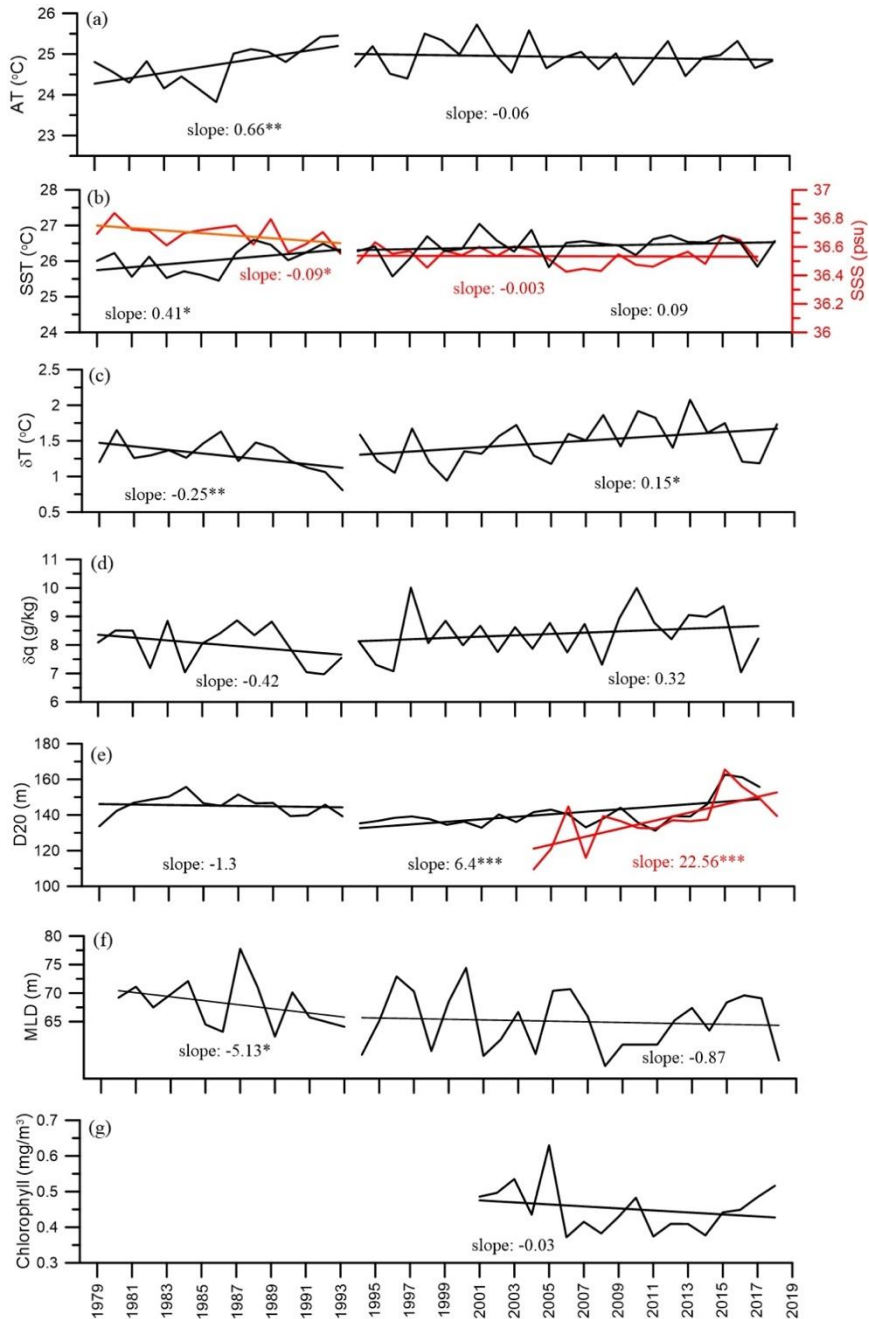


Figure S3: Same as in Figure S1 for the month of January. Corresponding slopes and p-values are given for each trendline. ***, **, * represents $p < 0.01, 0.05, 0.1$ respectively

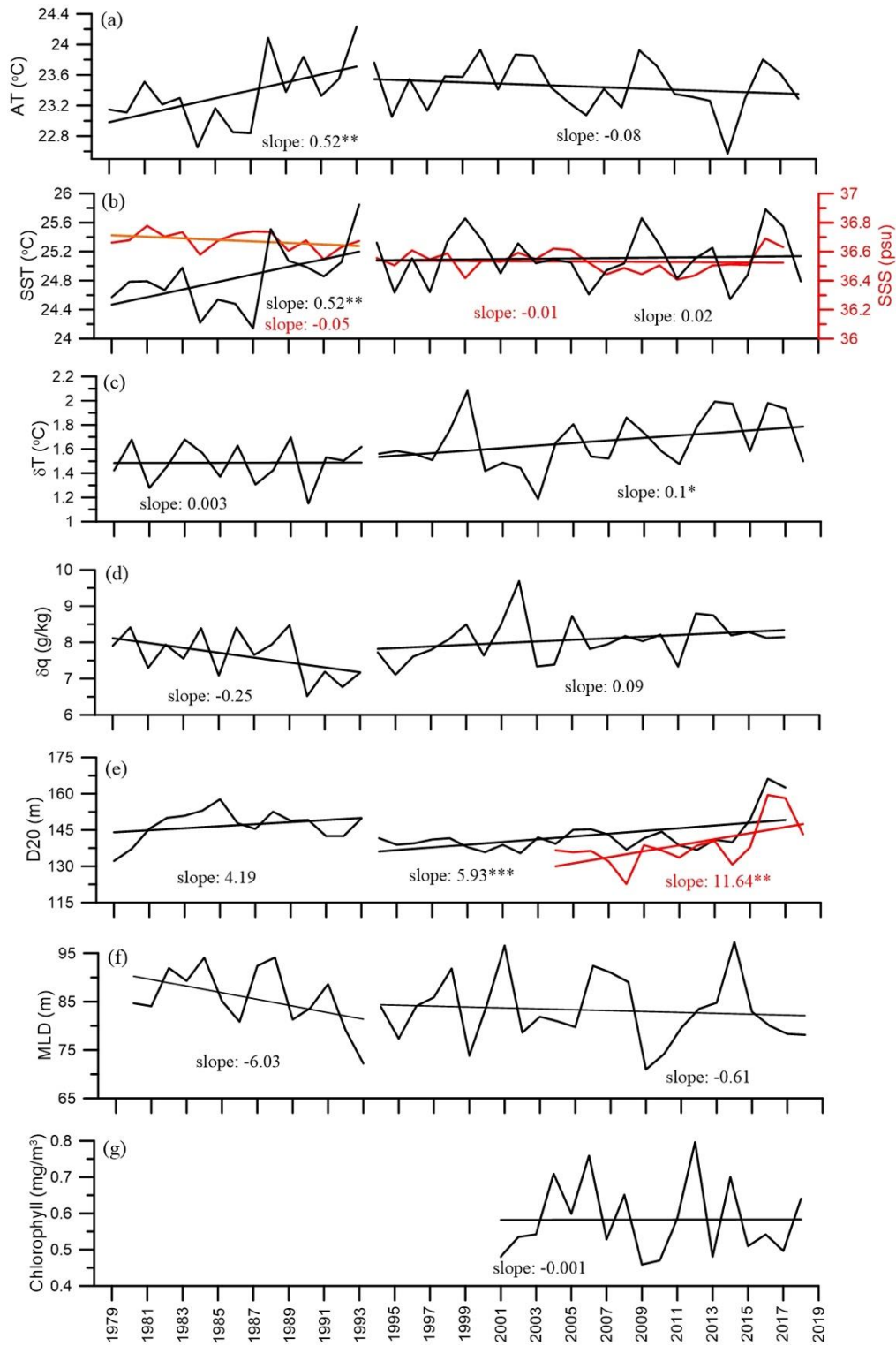


Figure S4: Same as in Fig. S1 for the month of February. Corresponding slopes and p-values are given for each trendline. ***, **, * represents $p < 0.01$, 0.05 , 0.1 respectively

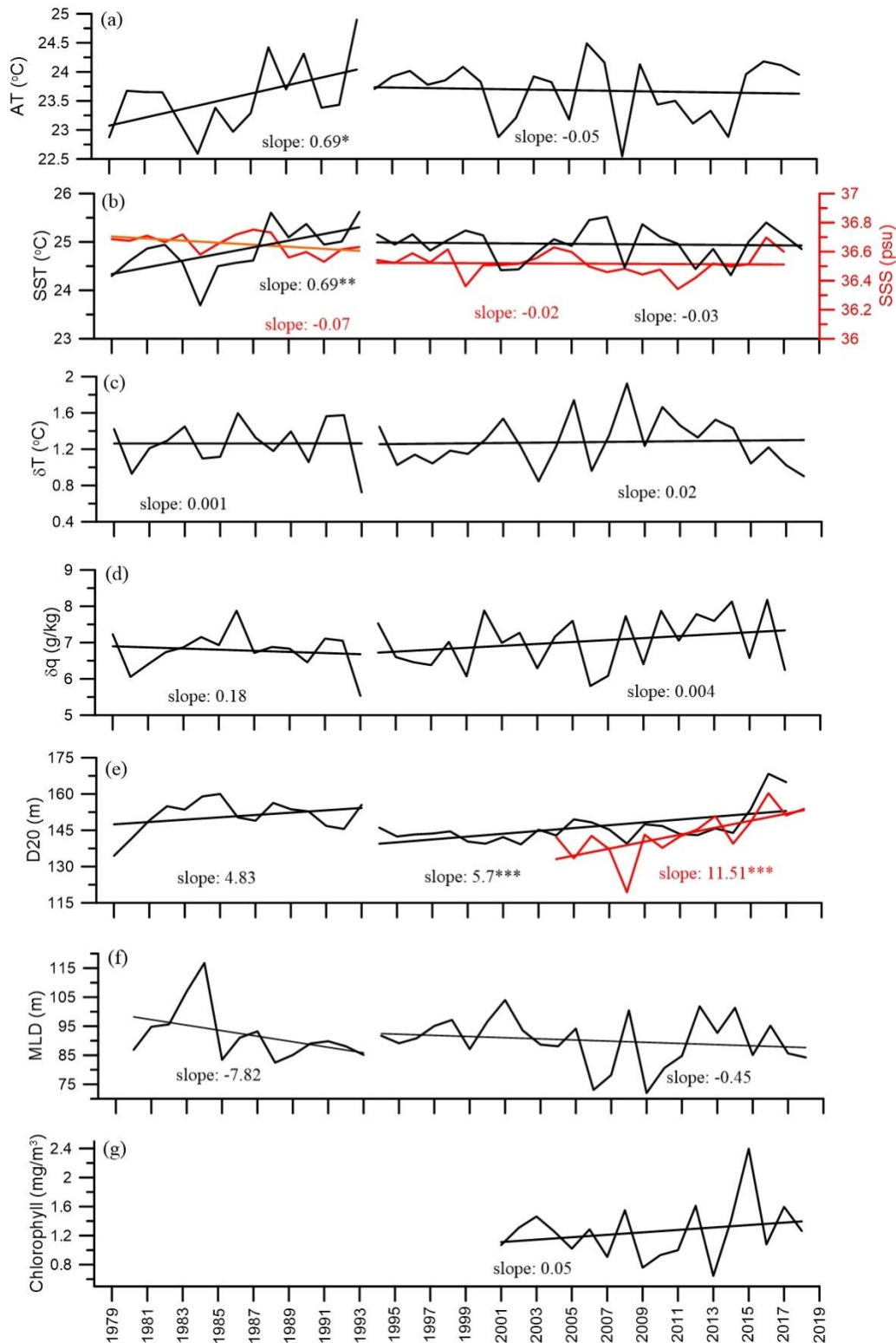


Figure S5: Long term spatial trends of chl-a (mg/m³/y) in the Arabian Sea

